

## Article

# Early Detection of Failing Lead-Acid Automotive Batteries Using the Detrended Cross-Correlation Analysis Coefficient

Thiago B. Murari <sup>1,\*</sup>, Roberto C. da Costa <sup>2</sup>, Hernane B. de B. Pereira <sup>1,3</sup>, Roberto L. S. Monteiro <sup>1,4</sup>  
and Marcelo A. Moret <sup>1,5</sup>

<sup>1</sup> Departamento de Modelagem Computacional, Universidade SENAI CIMATEC, Salvador 41650-010, BA, Brazil; hbbpereira@gmail.com (H.B.d.B.P.); robertolsmonteiro@gmail.com (R.L.S.M.); mamoret@gmail.com (M.A.M.)

<sup>2</sup> Stoneridge Electronics AB, Gustav III:s Boulevard 26, 169 73 Solna, Sweden; rccosta@gmail.com

<sup>3</sup> Departamento de Educação, Universidade do Estado da Bahia—UNEB, Salvador 41150-000, BA, Brazil

<sup>4</sup> Departamento de Ciências Exatas e da Terra, Universidade do Estado da Bahia—UNEB, Alagoinhas 48000-000, BA, Brazil

<sup>5</sup> Departamento de Ciências Exatas e da Terra, Universidade do Estado da Bahia—UNEB, Salvador 41150-000, BA, Brazil

\* Correspondence: thiago.murari@fieb.org.br

**Abstract:** This work introduces a model for lead-acid battery health monitoring in automobiles, focusing on detecting degradation before complete failure. With the proliferation of electronic modules and increasing power demands in vehicles, along with enhanced sensor data availability, this study aims to investigate battery lifespan. Dead batteries often lead to customer dissatisfaction and additional expenses due to inadequate diagnosis. This study seeks to enhance predictive diagnostics and provide drivers with timely warnings about battery health. The proposed method employs the Detrended Cross-Correlation Analysis Coefficient for end-of-life detection by analyzing the cross-correlation of voltage signals from batteries in different states of health. The results demonstrate that batteries with a good state of health exhibit a coefficient consistently within the statistically significant cross-correlation zone across all time scales, indicating a strong correlation with reference batteries over extended time scales. In contrast, batteries with a deteriorated state of health compute a coefficient below 0.3, often falling within the non-significant cross-correlation zone, confirming a clear decline in correlation. The method effectively distinguishes batteries nearing the end of their useful life, offering a low-computational-cost alternative for real-time battery monitoring in automotive applications.

**Keywords:** lead-acid battery; state of health; automotive;  $\rho$ DCCA



Academic Editor: Hal Gurgenci

Received: 9 November 2024

Revised: 8 February 2025

Accepted: 19 February 2025

Published: 28 February 2025

**Citation:** Murari, T.B.; Costa, R.C.d.; Pereira, H.B.d.B.; Monteiro, R.L.S.; Moret, M.A. Early Detection of Failing Lead-Acid Automotive Batteries Using the Detrended Cross-Correlation Analysis Coefficient. *Appl. Syst. Innov.* **2025**, *8*, 29. <https://doi.org/10.3390/asi8020029>

**Copyright:** © 2025 by the authors. Published by MDPI on behalf of the International Institute of Knowledge Innovation and Invention. Licensee MDPI, Basel, Switzerland. This article is an open access article distributed under the terms and conditions of the Creative Commons Attribution (CC BY) license (<https://creativecommons.org/licenses/by/4.0/>).

## 1. Introduction

The use of motor vehicles is common in people's daily lives, allowing for transportation to work or leisure, whether planned or in emergencies. One of the fundamental points for the beginning of this journey is to start the car.

When analyzing the simplified operation of the system, the starter motor of the car, plugged in a lead-acid battery, allows the combustion engine to start rotating. The engine control module coordinates fuel injection and controls sparks in the engine cylinders, and the energy generated by internal combustion keeps the engine running. At this moment, the starter motor can be deactivated [1] and the alternator starts to convert the rotation of the engine shaft into voltage and electrical current, allowing the system to remain stable and the lead-acid battery also to be recharged [2].

There have been few changes in automotive lead-acid batteries technology over the past 90 years. With respect to design and manufacturing process technologies, batteries are expected to have an average lifespan ranging from 2 to 7 years (depending on climatic conditions), reliability and robustness, cold start capacity, and the ability to meet all these requirements with minimal material consumption, weight, and cost [2].

Despite having a relatively low energy density, only 30 to 40% of the conceptual limit when compared to 90% for lithium-ion batteries, lead-acid batteries are advantageous due to their use of abundant, nonflammable, and low-cost materials, and water-based electrolyte. Additionally, manufacturing practices with a 99% recycling rate significantly minimize their environmental impact [3,4].

If the starter motor does not function properly, one of the possible causes is malfunction of the lead-acid battery. The battery undergoes wear over time, until a moment when it ceases to serve its primary function [5]. To monitor the state of a battery, many automakers use sensors in close proximity. This sensor setup is known as the Battery Monitor Sensor (BMS) [1], which typically monitors current, temperature, and battery voltage. In some applications, the BMS is positioned directly on the negative terminal of the battery and communicates through a Local Interconnect Network protocol with an Engine Control Module, in some cases with the Body Control Module (BCM) of the vehicle.

An automotive battery is a complex nonlinear electrochemical process for which behavior analysis is needed to determine its usage conditions, such as the State of Charge (SOC) and State of Health (SOH). From this battery data acquisition by the BMS and sharing with the BCM, several control strategies have been developed and implemented, such as inferring the SOC of the battery from a combination of the voltage and the delta of the current entering and leaving the battery. The SOH is calculated as the ratio of the actual cell capacity resistance to its initial value [6–8].

Nowadays, innovations and cutting-edge advancements in renewable energy conversion are transforming global energy systems, such as hybrid electric vehicles (HEVs) and renewable electricity generation, to significantly decrease reliance on fossil fuels [9]. Despite the widespread adoption of lithium-ion batteries in HEVs, lead-acid batteries have remained the predominant electrochemical power source for medium-to-large energy storage applications since their development [10].

Lead-acid batteries are required to operate under partial state of charge conditions for renewable energy storage and HEV applications, but a specific failure mode known as sulfation degrades their capacity and performance [11]. To address this challenge, a new technology called Lead-Carbon Batteries has emerged, incorporating functional carbon additives into the negative active material to raise the performance of traditional lead-acid batteries [12].

Another current application of lead-acid batteries is in electric two-wheeler vehicles (E2Ws), which are equipped with electric motors rated for continuous power between 0.25 and 4 kW, have a top speed of 45 km/h, and require approximately 8 h to charge. These vehicles are overwhelming sold in Asian markets, particularly in China and Vietnam [13]. E2Ws are regarded as significantly more energy efficient than their petrol-based counterparts, consuming three to five times less energy than gasoline-powered two-wheelers [14]. For lower-income countries, E2Ws present an attractive alternative, as they are more affordable compared to gasoline cars. With prices starting from around EUR 100 [15], E2Ws provide an economical and sustainable transportation option, making them especially appealing in regions where cost is a critical factor in purchasing decisions.

There have always been complaints about batteries failing without prior notice to the driver. Battery degradation is natural and expected, but the lack of information provided by the monitoring system can make this event a major issue for the driver [16]. This work's

main objective is to propose a go/no-go test for the SOH of lead-acid batteries. Our hypothesis is that batteries with deteriorated SOH exhibit a decay in cross-correlation with batteries in good SOH when analyzed across multiple time scales. This diagnostic method, based on the Detrended Cross-Correlation Analysis Coefficient (DCCAC), aims to identify this correlation decay, providing a clear indication of whether a battery remains in good condition or is nearing the end of its useful life. This approach helps drivers avoid unexpected failures and plan timely replacements.

## 2. Methods and Models for Evaluating Battery SOH Literature Review

Firstly, an analysis of methods and models for evaluating the health of a vehicle battery was developed based on the current literature. A search was conducted in the ScienceDirect, Springer, and IEEE repositories using the terms (SoH OR “State of Health”) AND “Lead-Acid Battery” AND (automotive OR vehicle). A total of 431 research articles, 161 review articles and 81 book chapters were obtained from ScienceDirect, 31 articles from Springer Link, and 21 articles from IEEE. Subsequently, some terms were considered for the removal of documents: items related to lithium-ion batteries, stationary usage batteries, solar energy applications, or purely electric vehicles batteries. Thus, this work presents the main findings identified in articles published since 2003.

Hariprakash et al. [17] reported that electrochemical sparse-impedance spectroscopy has proven to be an effective technique for assessing the SOH of sealed automotive lead-acid batteries, as it enables onboard data collection within the vehicle. They predicted that sparse-impedance spectroscopy could be increasingly applied in future vehicles to monitor the SOH of lead-acid battery systems.

A proposal was presented by May [18] for monitoring batteries under stop-start conditions, which included monitoring the SOC, SOH, open circuit voltage, voltage drop during startup, and voltage response to small loads. They concluded that the SOC and SOH are critical for achieving reliability standards. Similarly, Blank et al. [19] used the current and calculation of voltage ripples acquired with an electrochemical impedance spectroscopy meter across different frequency ranges to perform battery prognostics, concluding that impedance measurement is an effective tool for assessing battery states.

In the study presented by Okoshi et al. [20], the focus was on improving the accuracy of SOC inference by utilizing Direct Current Resistance (DCR), thereby enhancing the correlation between the SOC and DCR. Zhang et al. [21] monitored the SOH of the battery during engine startup, introducing a new battery model that considered the internal resistance of the battery and the voltage drop during startup. This approach achieved better battery diagnostic performance compared to the conventional method at the time, which was based on resistance. They also suggested the use of detection methods with statistical models for future research.

Ushiyama and Masayuki [22] also focused their study on SOH estimates for lead-acid batteries, specifically by considering the waveforms of voltage and current at the battery terminals during operation. They produced their SOH estimates by analyzing changes in the battery’s internal resistance and capacitance. Aware of the limitations of SOH measurement by inference, Marcos et al. [23] proposed measuring the SOH and SOC through the electrolyte density, using an optical fiber inserted into the battery. However, a downside of this research, when compared to the study in this dissertation, is that it requires an invasive method to obtain and measure the electrolyte density.

Li et al. [24] proposed an approach for estimating the SOC and SOH using a dynamic data-driven method, applying Symbolic Dynamic Filtering along with a D-Markov machine and a Probabilistic Finite State Automaton. It considered the current and voltage as parameters in a time series, resulting in a dynamic data-driven method as an alternative to

traditional battery model-based methods. Li et al. [25] also presented a study involving battery current time series alongside voltage, which can be considered a continuation of the previous research presented in [24].

Kerley et al. [26] presented a system for measuring the SOH based on the battery's voltage drop curve during a startup event, monitoring the first two voltage drops over time, along with the battery's temperature and the SOC. The algorithm developed can raise warnings of battery SOH deterioration, but it still needs improvements to increase system reliability. This application was tested in a controlled environment. For future research, Kerley et al. [26] suggested applying the algorithm in real-world scenarios, along with field tests.

In the article presented by Piłatowicz et al. [27], a model based on the Butler–Volmer equation was introduced, capable of accurately predicting the battery's voltage response across a wide range of discharge currents, SOC, and temperatures. The model successfully predicted the battery's voltage drop even in a dynamic environment with varying electrical loads and operating conditions, including scenarios with low battery SOC.

Hyun [28] proposed a method for estimating battery SOH during the startup phase, using only the SOC, battery temperature, and the voltage drop from the resting state to the first voltage dip, as well as between the first and second voltage dips. The result was a system capable of estimating the SOH without the need for a current sensor installed in the vehicle.

In the work presented by Bressanini et al. [29], a design and implementation of an SOH and SOC estimator model were presented. The SOH estimation was based on the battery's internal resistance, while the SOC was determined using the Coulomb counting method during the battery's charge and discharge phases. For SOC estimation, the measurements considered the currents entering and exiting the battery, while the SOH was assessed during the initial charging stages of the battery. Kwiecien et al. [30] provided an overview indicating that automotive lead-acid battery technologies still face numerous challenges and are expected to continue evolving over the next two decades. They also highlighted the importance of battery sensors (BMS) for real-time monitoring of battery current, voltage, and temperature, along with the implementation of adaptive algorithms and high parameterization work as key paths for advancement. Kwiecien et al. [30] further suggested that determining the available battery capacity throughout its lifespan, which is directly related to the SOH, remains an unsolved issue.

Zhang et al. [31] presented a study with a focus on battery modeling. In this case, a distinction was made between the explanation of the thermal and electrical phenomena of the battery, as well as the evolution of major battery failures. This was followed by the application of a two-time-scale method in a model-based estimator. The algorithm in the broader time scale monitors the battery and adjusts the parameters of the model on the more immediate scale. It was concluded that the hybrid algorithm system was able to monitor the battery and continuously self-adjust over time.

From a hardware perspective, and with regard to the study of battery modeling, Kumar et al. [32] presented a battery SOC and SOH estimator based on a Neuro-Fuzzy approach and statistical models, implemented on a Field-Programmable Gate Array (FPGA) within a BMS. The model took into account the consumption time, electrical current drain, terminal voltage, temperature, and internal battery resistance. This study provided an alternative for BMS systems, highlighting advantages such as low non-recurring engineering costs, low power consumption, high processing speed, configurable logic, large storage capacity, and more flexible interfaces.

Wassiliadis et al. [33] developed Kalman filter studies by using an extended double Kalman Filter (KF) to estimate the SOC and SOH in a case study focused on battery life

cycle analysis. They used battery resistance and capacity estimates as parameters. The study concluded that this method is essential for improving model accuracy and enhancing the robustness of the filters, especially for aged batteries.

Further, Khaleghi et al. [34] proposed a data-driven algorithm under multiple conditions to estimate the SOH using known load applications. They used a driving cycle called the Worldwide Light Duty Driving Test Cycle in the laboratory to perform acquisitions simulating real-world usage. Indicators obtained through time and frequency domain measurements of the voltage and current over defined time intervals were used, allowing for real-time investigation of battery SOH degradation.

Li et al. [35] presented an article on a battery management system based on cloud processing, utilizing a Digital Twin for the SOH and SOC of the battery. The study considered a context where battery data would be available via the Internet of Things, making this initiative feasible. For this work, equivalent circuit models, electromechanical models, and machine learning models were used, with the pros and cons of each model being considered.

Calborean et al. [36] introduced a new approach using Electrochemical Impedance Spectroscopy to predict the lifespan of battery cells under specific aging conditions. Fluctuations were monitored during charge and discharge sequences at two SOC levels. By studying the resonance frequencies of the batteries during the aging process, a trend in the battery's SOH was identified.

Guida et al. [37] proposed the ERMES algorithm which offers a robust and computationally efficient method for real-time estimation of a battery's SOC and SOH, addressing the challenges posed by complex and time-varying battery dynamics. A key feature of ERMES is its ability to capture sudden SOH variations based on a simple battery model, with potential for extension to other parameters. The algorithm also provides a figure of merit, called the SOU, which measures the accuracy of its estimates, allowing for real-time monitoring of its robustness. If prediction uncertainty exceeds a certain threshold, the system can dynamically adjust the model composition, such as by fine-tuning parameters or adding models close to the current SOH estimate.

In summary, there are several algorithms used for the estimation of the SOC and SOH of batteries. The voltage method for estimating the SOC involves measuring the open-circuit voltage of the battery and then comparing it to either a lookup table or a mathematical model. Although this approach is noninvasive, it is susceptible to fluctuations in temperature and the evolving nature of battery aging [29,38,39]. The Coulomb counting method estimates the SOC by integrating the current flowing in and out of the battery. Although this method is simple to implement, it is vulnerable to cumulative errors stemming from inaccuracies in measurements, parasitic currents, and variations in battery capacity due to temperature and aging fluctuations [40–42]. The KF approach utilizes a recursive filter algorithm along with a comprehensive mathematical model of the battery. While offering a more precise estimation of the SOC when compared to other methods such as Coulomb counting and voltage estimation [43], this approach requires substantial computational resources, constraining its practicality in resource-limited applications, especially in the automotive sector [33,44].

The Neural Network method involves training a neural network using a dataset of batteries measurements to establish a correlation between input parameters (such as the ampere, temperature, and voltage) and the SOC. Subsequently, the neural network is employed to forecast the SOC or SOH based on real-time or historical battery data [45,46]. However, the effective deployment of this algorithm heavily depends on the presence of a sizable and varied dataset for training the neural network, along with a remarkable computational resources for both training and inference tasks [47].

Jiang and Song ([46]) provided an extensive evaluation and comparison of different methods for analyzing the SOH of batteries. An ideal SOH estimation method that can be applied in any charging or discharging situation, and can be used quickly, accurately, and economically, does not exist yet. However, the KF method and its variants, along with data-driven methods or a combination of these two types of methods, appear to be the most promising candidates for achieving the best possible SOH estimation.

The KF method and its variants have been proven effective in state of charge (SOC) estimation under complex working conditions, and can at least provide a rough estimate of battery SOH online. However, the accuracy of these methods in SOH estimation requires further testing, and the selection of different KF variants to balance estimation accuracy and computational cost needs additional study. For data-driven methods, some quick and accurate SOH estimations have been achieved, but the challenge remains in extracting features closely related to the battery's SOH from data obtained under irregular charging and discharging conditions [46].

### 3. Materials and Method

#### 3.1. Data Acquisition and Vehicle Setup

For data acquisition, a PicoScope 2204A digital oscilloscope from the 2000 series was used, with a bandwidth of 10 MHz and 8-bit resolution at 100 MS/s, connected to a laptop running the PicoScope 6 application, version 6.14.23.5207. The probe tip was positioned directly on the battery terminals for voltage acquisition. The setup used for acquisitions was  $\pm 20$  V and 100 ms/div, with a trigger for voltage drops below 10 V. The sampling rate in the BMS-BCM system available in vehicles was adjusted to 1ms per point.

Following the instrumentation, a Vehicle Start and Stop procedure was performed. At this stage, battery rest was preconditioned for at least 12 h with the vehicle at rest after use. During this stage, the voltage time series data to be evaluated were collected. All data were collected at the same time of day, on a single day in an indoor environment, ensuring conditions without significant changes in equipment temperature. The collected data were filtered to display only the area of interest, keeping the initial point of all measurements aligned at the same moment, i.e., the zero point before voltage drops, allowing monitoring of each millisecond of the measurements while maintaining the same length of the time series. It is important to define the length of the time series, because a finite number of records can introduce unacceptable fluctuations and bias in statistical calculations. To ensure reliable analysis, our final dataset consists of 1193 points per vehicle, which provides a sufficient number of data points to capture the voltage behavior up to a stable reference point in the graph.

The tested vehicles were as follows:

- Y1.1 = Subcompact car, 1.5 L engine, with 1 month of battery usage
- Y1.2 = Subcompact car, 1.5 L engine, with 6 months of battery usage
- Y1.3 = Subcompact car, 1.5 L engine, with 32 months of battery usage
- Y2.1 = Compact car, 2.0 L engine, with 15 months of battery usage
- Y2.2 = SUV car, 2.0 L engine, with deteriorated SOH
- Y2.3 = SUV car, 2.0 L engine, where the original battery was replaced by an aftermarket battery. Aftermarket battery with 6 months of usage
- Y2.4 = SUV car, 2.0 L engine, with deteriorated SOH. The battery received a new charge before the measurement

The starter motor system and engine are the same for the Compact (Y2.1) and SUV (Y2.2, Y2.3, and Y2.4) vehicles. During the data acquisition and subsequent filtering of voltage time series, it was possible to obtain the set of curves presented in Figure 1. A voltage drop can be observed at the moment of starting, which is particularly pronounced

in batteries with deteriorated SOH. In vehicles Y2.2 and Y2.4, the initial voltage dip was not only deeper but also took longer to recover, indicating a reduced capacity to supply the necessary current. Comparatively, vehicles Y1.1 and Y2.1, which served as baselines, exhibited a more stable voltage profile, with a faster recovery to nominal voltage values. This suggests that the ability of a battery to maintain voltage under load conditions is directly correlated with its SOH. Additionally, the oscillations observed in the voltage time series for vehicles with degraded batteries may indicate increased internal resistance and reduced charge retention capacity. As the engine starts, the voltage tends to increase until the voltage returns above 12 volts, which is characteristic of a functioning combustion engine.

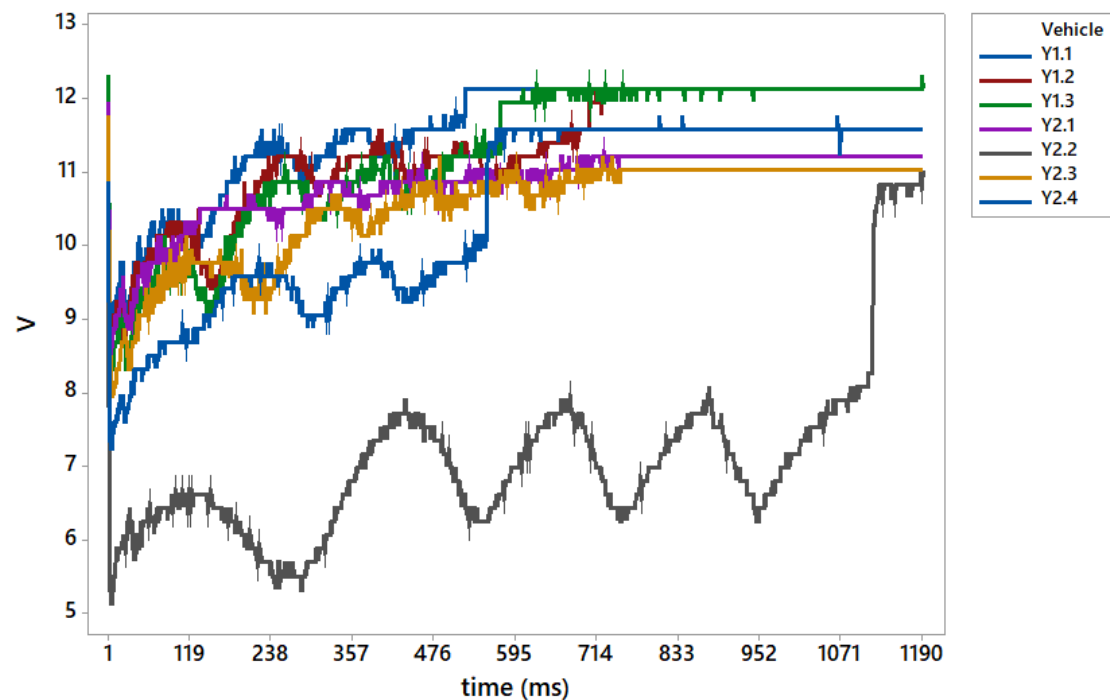


**Figure 1.** Filtered data collected for the 7 vehicles. The axis Y is the measured voltage (V) in each vehicle and the axis X is the time in milliseconds.

### 3.2. Detrended Cross-Correlation Analysis Coefficient

The DCCAC was first introduced and implemented by Zebende [48]. It uses detrended fluctuation analysis (DFA) [49] and detrended cross-correlation analysis (DCCA) [50] to measure the degree of cross-correlation. These methods have been applied in mobility [51], biological processes [52], climate [53], econophysics [54–57], big data [58], and epidemic data series [59–61]. It provides an index for quantifying the cross-correlation between two nonstationary time series [62]. Examining these fluctuations enables the identification of co-movements between two time series.

Two studies may be highlighted regarding the application of DCCAC to evaluate different behaviors. Azevedo et al. [51] proposed a method to assess the impact of rainfall on bus accessibility for passengers with disabilities and the elderly compared to other passengers. Using the DCCAC, they identified the bus lines and city areas with the worst accessibility for PWD and elderly passengers during the rainy season. Dong and Gao [63] analyzed a twin-engine aircraft and found that the fuel flow time series from the left and right engines exhibited significantly stronger cross-correlations than the exhaust gas temperature time series from the same engines.

Compared to Pearson's method, the DCCAC is more robust to contaminated noises and less sensitive to the amplitude ratio between slow and fast components [64]. This is an efficient correlation coefficient used to estimate correlations between non-stationary

time series. The method also follows the procedure of [65] to test the significance of the correlation and calculate the 95% confidence intervals for non-significant results.

DCCAC is calculated using the following equations [48]:

Consider two paired time series,  $\{x_t\}$  and  $\{y_t\}$ , where  $t = 1, 2, \dots, N$ , with  $N$  representing the total length of the time series. To remove non-stationary trends and better analyze the cross-correlations between the two time series, the cumulative sum (integration) of each series is computed to obtain two new integrated time series, as shown in Equation (1).

$$xx_k = \sum_{t=1}^k x_t \quad \text{and} \quad yy_k = \sum_{t=1}^k y_t, \quad k = 1, 2, \dots, N \quad (1)$$

Next, the integrated time series  $\{xx_k\}$  and  $\{yy_k\}$  are divided into overlapping boxes of equal length  $s$ . The number of overlapping boxes is given by  $(N - s)$ , and the box length  $s$  is constrained within the range  $4 \leq s \leq \frac{N}{4}$ .

Within each box, the local trend of the time series is estimated using a least-squares polynomial fit, denoted as  $xP_i(k)$  for  $\{xx_k\}$  and  $yP_i(k)$  for  $\{yy_k\}$ . The residuals from these local trends represent detrended fluctuations, which are used to compute the covariance of residuals within each box, as given by Equation (2).

$$f^2_{xy}(s, i) = \frac{1}{s + 1} \sum_{k=1}^{i+s} (xx_k - xP_i(k))(yy_k - yP_i(k)) \quad (2)$$

To obtain a global measure of covariance across all overlapping boxes, the average of the covariance over all boxes is computed, yielding the detrended covariance function, as shown in Equation (3).

$$F^2_{xy}(s) = \frac{1}{N - s} \sum_{i=1}^{N-s} f^2_{xy}(s, i) \quad (3)$$

Finally, the Detrended Cross-Correlation Analysis Coefficient (DCCAC) is determined using Equation (4). The DCCAC normalizes the covariance function by the individual detrended fluctuation functions  $F_{xx}(s)$  and  $F_{yy}(s)$ , which represent the auto-affinity of each time series.

$$DCCAC(s) = \frac{F^2_{xy}(s)}{F_{xx}(s)F_{yy}(s)} \quad (4)$$

The DCCAC is a dimensionless coefficient. Its value ranges between  $-1$  and  $+1$ , where:

- DCCAC =  $+1$ : the time series are perfectly cross-correlated;
- DCCAC =  $0$ : indicates no cross-correlation between the two analyzed time series;
- DCCAC =  $-1$ : the time series are perfectly anti-correlated.

By applying this method to battery voltage time series, it becomes possible to quantify how the cross-correlation strength varies across multiple time scales, allowing for an effective comparison of batteries with good and deteriorated SOH.

### 3.3. Interpreting DCCAC Results for Battery SOH Evaluation

In the context of battery SOH evaluation, DCCAC allows for the comparison of voltage signals from a battery under test with a reference battery in good condition. The main hypothesis is that batteries with deteriorated SOH exhibit a decay in correlation with healthy batteries across multiple scales. By analyzing this behavior, it becomes possible to determine whether a battery is in good SOH condition or approaching failure.

When interpreting the DCCAC results, a battery with good SOH should exhibit a significant and increasing DCCAC value as the time scale increases, inside the zone B,

green color, presented in Figure 2. This indicates that the voltage signals maintain strong cross-correlation, which is expected for batteries operating under similar conditions. In contrast, batteries with degraded SOH show weaker correlation, with DCCAC values that remain low or statistically non-significant across different time scales, partially inside the zone A, grey color, presented in Figure 2. This pattern suggests a disruption in the expected voltage behavior during engine ignition.

Another key aspect of the analysis is the presence of results falling within the non-significant cross-correlation area. Batteries with severely deteriorated SOH tend to have most of their computed DCCAC values within this non-significant range, inside the zone A, grey color, presented in Figure 2. This means that their voltage signals do not exhibit a meaningful correlation with a healthy reference battery, reinforcing the conclusion that the battery is no longer performing optimally. The ability to distinguish between significant and non-significant cross-correlation is crucial for establishing a clear threshold for battery failure detection.

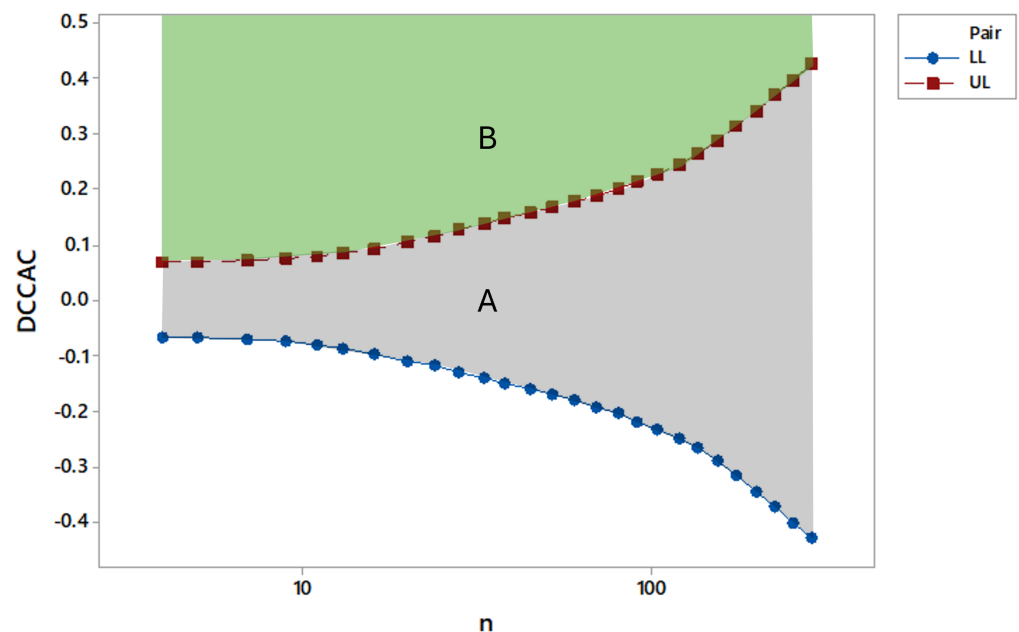


**Figure 2.** DCCAC results interpretation: Zone A is defined by the 95% confidence interval upper limit (UL) and 95% confidence interval lower limit (LL) and represents the statistically non-significant area, calculated using the method proposed by Podobnik et al. [65]. Zone B corresponds to the statistically significant area, where meaningful correlations can be observed. Batteries with good SOH should have all computed DCCAC results within Zone B, indicating significant cross-correlation with the reference battery.

#### 4. Results and Discussion

First, one baseline vehicle was selected for each engine displacement. Vehicles Y1.1 and Y2.1 presented the lowest MIS and the best battery SOH. Thus, vehicles with the same engine displacement were evaluated against the baseline vehicle. The DCCAC was calculated for the pairs Y1.1,Y1.2 and Y1.1,Y1.3 for 1.5L engine displacement. Pairs Y2.1,Y2.2, Y2.1,Y2.3, and Y2.1,Y2.4 were evaluated for 2.0L engine displacement.

Figure 3 shows the results for 1.5L engine displacement. All the batteries are in good SOH. The DCCAC for the pair Y1.1,Y1.2 exhibits a steady increase from 0.0613 at  $n = 4$  to 0.5880 at  $n = 285$ , indicating a progressively stronger correlation as the box size increases. This behavior was noticed in batteries operating under similar conditions. For the pair Y1.1,Y1.3, the DCCAC follows a similar trend but reaches a higher value of 0.8829 at

$n = 285$ , indicating a strong cross-correlation between these two vehicles. Despite the 32-month usage period of the Y1.3 battery, the results suggest that it retains a stable voltage profile comparable to that of a new battery. The highlight in Figure 3 is the pattern of the rising curve for batteries with good SOH, demonstrating how the cross-correlation strengthens from short- to long-term scales.

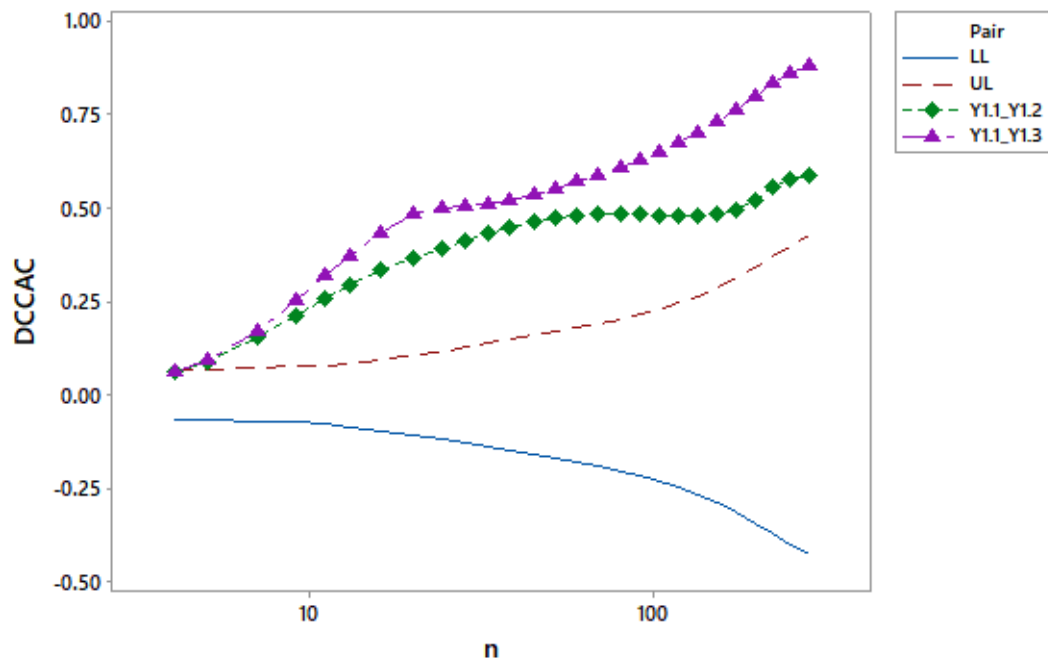


**Figure 3.** DCCAC of the following vehicle pairs: Y1.1,Y1.2 and Y1.1,Y1.3. Vehicle Y1.1 is the baseline for this analysis. The 95% confidence interval upper limit (UL) and 95% confidence interval lower limit (LL) are also presented.

The results for 2.0L engine displacement are presented in Figure 4. Only the baseline and Y2.3 vehicles have batteries in good condition of use, with adequate SOH. The DCCAC increases from 0.0210 at  $n = 4$  to 0.7263 at  $n = 285$  for the Y2.1,Y2.3 pair. The pair Y2.1,Y2.2 and Y2.1,Y2.4, both featuring vehicles with deteriorated SOH, present weak and statistically non-significant DCCAC values across all time scales. Even in the case of Y2.4, where the battery was recently recharged, the DCCAC remains low. This suggests that recharging a battery with degraded SOH does not restore its ability to sustain voltage stability under load. The lack of significant correlation in these cases highlights a fundamental deterioration in battery performance, further reinforcing the effectiveness of DCCAC in identifying failing batteries. In contrast, the rising curve trend seen in Figure 3 is also observed in Figure 4 for the pair Y2.1,Y2.3, reinforcing that batteries with good SOH maintain a consistent and increasing cross-correlation coefficient from short- to long-term scales.

Finally, it was verified that the method cannot be applied to compare different engine displacements using a unique baseline engine as a reference. Figure 5 evaluates the pairs Y2.1,Y1.2 and Y2.1,Y1.3 against the 95% confidence intervals. Vehicle Y2.1, with a 2.0-L engine, serves as the baseline for this analysis, while Y1.2 and Y1.3 are 1.5 L engine vehicles with batteries in good SOH. Initially, DCCAC values for the pair Y2.1,Y1.2 are not statistically significant, as they fall between the UL and LL for almost all boxsizes. As the boxsize increases ( $n \geq 224$ ), DCCAC values exceed the UL, indicating statistically significant positive cross-correlation. For the pair Y2.1,Y1.3, DCCAC values are significant for smaller box sizes ( $n > 38$ ), but become statistically insignificant afterward, almost mimicking the other analyzed pair for the remaining box sizes. However, unlike the rising curves observed in

Figure 3, Figure 5 presents a break in the constant rising pattern, indicating that DCCAC comparisons between different engine displacements may be unfeasible.

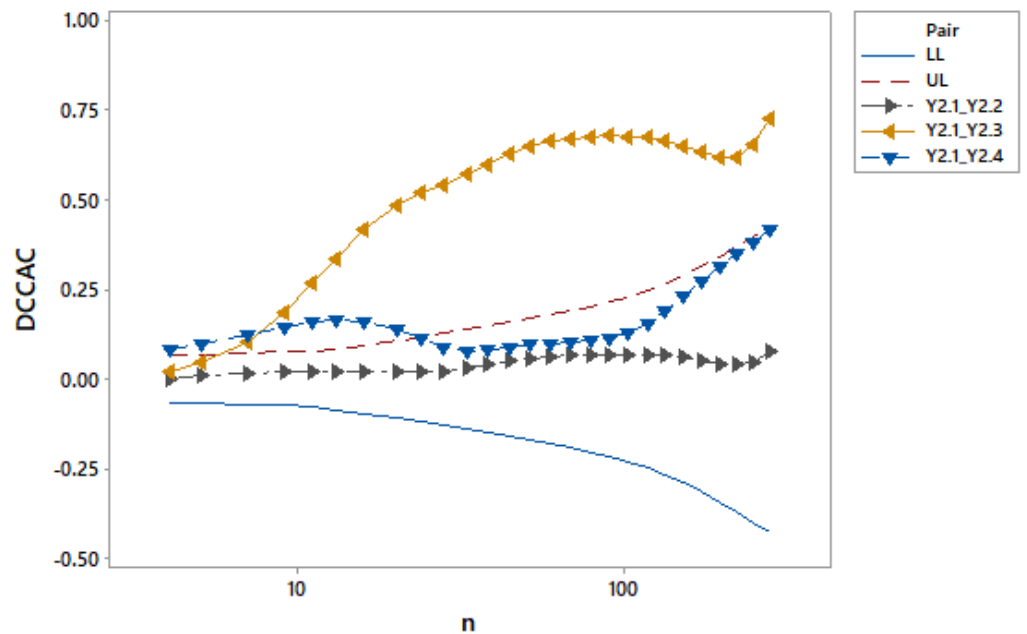


**Figure 4.** DCCAC of the following vehicle pairs: Y2.1,Y2.2; Y2.1,Y2.3 and Y2.1,Y2.4. Vehicle Y2.1 is the baseline for this analysis. The 95% confidence interval upper limit (UL) and 95% confidence interval lower limit (LL) are also presented.

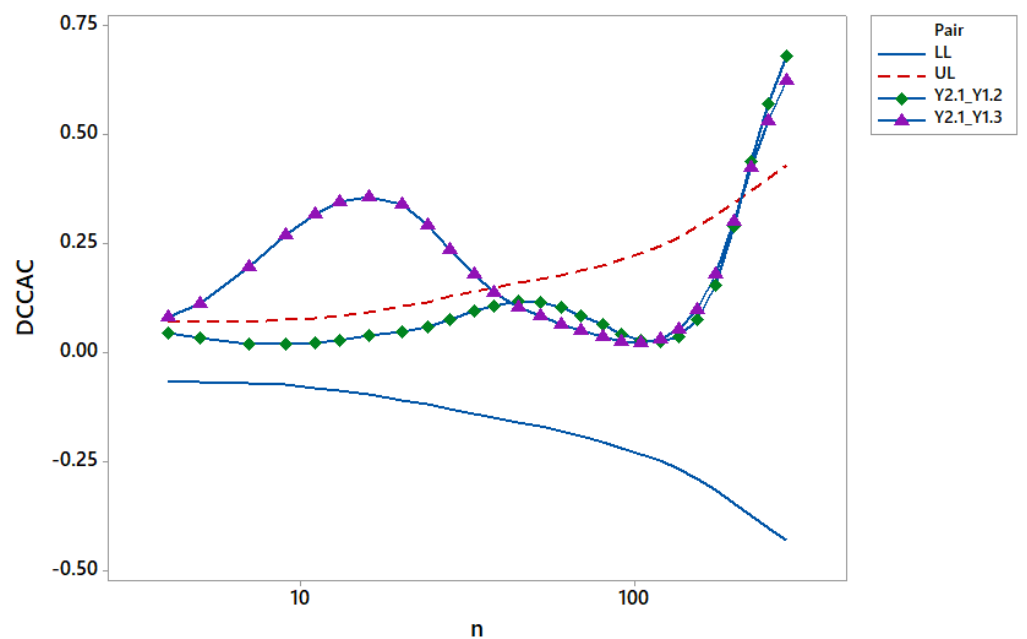


**Figure 5.** DCCAC of the following vehicle pairs: Y2.1,Y1.2 and Y2.1,Y1.3. Vehicle Y2.1 is the 2.0 L engine baseline for this analysis, and Y1.2 plus Y1.3 are 1.5 L engine vehicles with batteries with good SOH. The 95% confidence interval upper limit (UL) and 95% confidence interval lower limit (LL) are also presented.

Overall, a vehicle with a battery with adequate SOH will present significant DCCAC values across all box sizes  $n$  when compared to the baseline vehicle. The coefficient increases for long-term boxes, creating a rising pattern for the curve. A battery with deteriorated SOH will present DCCAC values that are weak or statistically non-significant for both

short- and long-term boxes when compared to those of the baseline vehicle with a battery in good SOH. DCCAC is a simple method to implement, with low computational cost, and can be used as a vehicle feature to identify deteriorated SOH before the battery is completely dead and the engine cannot start.

## 5. Conclusion

This work applied the DCCAC method to evaluate the SOH of lead-acid batteries using a time series of voltage measurements during vehicle start-up. A comparison of a battery with SOH deterioration and one without signs of deterioration, within the same engine displacement, did not show a statistically significant cross-correlation, while comparisons between batteries with an adequate SOH state showed a statistically significant cross-correlation across the size boxes of time. This difference in behavior allowed for the segregation of batteries with adequate SOH from those with deteriorated SOH, nearing the end of their useful life, even though the battery is still capable of starting the combustion engine.

This approach may offer advantages over other SOH estimation methods in the literature. It does not require complex modeling, extensive datasets, or high computational resources, making it an efficient, cost-effective solution for real-time battery monitoring in automotive systems. The DCCAC method can be integrated into vehicles to identify deteriorating SOH before the battery reaches critical failure levels, offering drivers a preemptive alert and allowing better maintenance planning.

An essential step in comparing a battery with a good SOH to one with a deteriorated SOH is the calculation of the statistically non-significant zone. This step is crucial as it enables a meaningful comparison of results and helps define the critical region for the cross-correlation index. By establishing this zone, it becomes possible to accurately identify the thresholds where the cross-correlation index indicates potential concern regarding battery health.

When compared to lithium-ion batteries, 12 V lead-acid batteries continue to hold a significant share in the global market. However, their challenges in operating efficiently under high-rate partial state of charge conditions make them less suitable for use in EVs. And in HEVs, the DCCAC needs to be tested and analyzed before it can be considered able to monitor battery degradation under partial state-of-charge conditions, a critical factor for ensuring optimal performance and longevity in energy storage applications. An option may be the usage of the method in E2Ws, which rely heavily on efficient and affordable lead-acid battery systems, where DCCAC offers a low-cost, computationally efficient approach to identify battery deterioration before the critical failure occurs.

Despite being used for the last few decades as an energy storage technology, lead-acid batteries will continue to play a crucial role in the global rechargeable battery market, offering significant advantages in terms of cost-effectiveness and recyclability. Future research should focus on expanding the application of DCCAC to different types of batteries, such as lead-carbon batteries, as well as integrating this method with other diagnostic tools to enhance predictive accuracy. It may also work with lithium-ion batteries, but new studies require to be conducted to confirm it. Real-world testing across various environmental conditions and usage patterns will help refine the method, potentially leading to improved models for predicting battery SOH across broader contexts. This work presents a new direction for improving battery health monitoring in the automotive industry.

**Author Contributions:** Conceptualization, T.B.M., R.C.d.C., and M.A.M.; methodology, T.B.M. and M.A.M.; software, R.C.d.C.; validation, R.C.d.C. and T.B.M.; formal analysis, T.B.M.; investigation, R.C.d.C.; resources, M.A.M.; data curation, R.C.d.C.; writing—original draft preparation, T.B.M., R.C.d.C., R.L.S.M., H.B.d.B.P., and M.A.M.; writing—review and editing, T.B.M., R.C.d.C., R.L.S.M., H.B.d.B.P., and M.A.M.; visualization, R.C.d.C., R.L.S.M., H.B.d.B.P., and M.A.M.; supervision, T.B.M.; project administration, T.B.M.; funding acquisition, M.A.M. All authors have read and agreed to the published version of the manuscript.

**Funding:** The authors acknowledge the funding provided by Conselho Nacional de Desenvolvimento Científico e Tecnológico (305096/2022-2).

**Institutional Review Board Statement:** Not applicable.

**Informed Consent Statement:** Not applicable.

**Data Availability Statement:** Data are available upon request.

**Conflicts of Interest:** Author Roberto C. da Costa was employed by the company Stoneridge Electronics AB. The remaining authors declare that the research was conducted in the absence of any commercial or financial relationships that could be construed as a potential conflict of interest.

## References

1. Chumchal, C.; Kurzweil, D. Lead–acid battery operation in micro-hybrid and electrified vehicles. In *Lead-Acid Batteries for Future Automobiles*; Elsevier: Amsterdam, The Netherlands, 2017; pp. 395–414.
2. Gelbke, M.; Mondoloni, C. Flooded starting-lighting-ignition (SLI) and enhanced flooded batteries (EFBs): State-of-the-art. In *Lead-Acid Batteries for Future Automobiles*; Elsevier: Amsterdam, The Netherlands, 2017; pp. 149–184.
3. Feldman, I.; Lifset, R.; Ellis, T.; Rifer, W.; Feldman, R.D. The circular economy: Regulatory and commercial law implications. *Envtl. L. Rep. News Anal.* **2016**, *46*, 11009.
4. Lopes, P.P.; Stamenkovic, V.R. Past, present, and future of lead–acid batteries. *Science* **2020**, *369*, 923–924. [[CrossRef](#)]
5. Culpin, B.; Rand, D. Failure modes of lead/acid batteries. *J. Power Sources* **1991**, *36*, 415–438. [[CrossRef](#)]
6. Khare, N.; Chandra, S.; Govil, R. Statistical modeling of SoH of an automotive battery for online indication. In Proceedings of the INTELEC 2008–2008 IEEE 30th International Telecommunications Energy Conference, San Diego, CA, USA, 14–18 September 2008; pp. 1–7. [[CrossRef](#)]
7. Dini, P.; Colicelli, A.; Saponara, S. Review on Modeling and SOC/SOH Estimation of Batteries for Automotive Applications. *Batteries* **2024**, *10*, 34. [[CrossRef](#)]
8. Li, Y.; Liu, K.; Foley, A.M.; Zülke, A.; Berecibar, M.; Nanini-Maury, E.; Van Mierlo, J.; Hoster, H.E. Data-driven health estimation and lifetime prediction of lithium-ion batteries: A review. *Renew. Sustain. Energy Rev.* **2019**, *113*, 109254. [[CrossRef](#)]
9. Moseley, P.T.; Rand, D.A.; Monahov, B. Designing lead–acid batteries to meet energy and power requirements of future automobiles. *J. Power Sources* **2012**, *219*, 75–79. [[CrossRef](#)]
10. Kurzweil, P. Gaston Planté and his invention of the lead–acid battery—The genesis of the first practical rechargeable battery. *J. Power Sources* **2010**, *195*, 4424–4434. [[CrossRef](#)]
11. Sajjad, M.; Zhang, J.; Zhang, S.; Zhou, J.; Mao, Z.; Chen, Z. Long-life lead-carbon batteries for stationary energy storage applications. *Chem. Rec.* **2024**, *24*, e202300315. [[CrossRef](#)] [[PubMed](#)]
12. Yin, J.; Lin, H.; Shi, J.; Lin, Z.; Bao, J.; Wang, Y.; Lin, X.; Qin, Y.; Qiu, X.; Zhang, W. Lead-Carbon Batteries toward Future Energy Storage: From Mechanism and Materials to Applications. *Electrochem. Energy Rev.* **2022**, *5*, 2. [[CrossRef](#)]
13. Rajper, S.Z.; Albrecht, J. Prospects of electric vehicles in the developing countries: A literature review. *Sustainability* **2020**, *12*, 1906. [[CrossRef](#)]
14. Majumdar, D.; Majumder, A.; Jash, T. Performance of low speed electric two-wheelers in the urban traffic conditions: A case study in Kolkata. *Energy Procedia* **2016**, *90*, 238–244. [[CrossRef](#)]
15. Weiss, M.; Dekker, P.; Moro, A.; Scholz, H.; Patel, M.K. On the electrification of road transportation—a review of the environmental, economic, and social performance of electric two-wheelers. *Transp. Res. Part Transp. Environ.* **2015**, *41*, 348–366. [[CrossRef](#)] [[PubMed](#)]
16. Mürken, M.; Kübel, D.; Thanheiser, A.; Gratzfeld, P. Analysis of automotive lead-acid batteries exchange rate on the base of field data acquisition. In Proceedings of the 2018 IEEE International Conference on Electrical Systems for Aircraft, Railway, Ship Propulsion and Road Vehicles & International Transportation Electrification Conference (ESARS-ITEC), Nottingham, UK, 7–9 November 2018; pp. 1–6. [[CrossRef](#)]

17. Hariprakash, B.; Martha, S.; Shukla, A. Monitoring sealed automotive lead-acid batteries by sparse-impedance spectroscopy. *J. Chem. Sci.* **2003**, *115*, 465–472. [[CrossRef](#)]
18. May, G. Valve-regulated lead-acid batteries for stop-and-go applications. *J. Power Sources* **2004**, *133*, 110–115. [[CrossRef](#)]
19. Blanke, H.; Bohlen, O.; Buller, S.; De Doncker, R.W.; Fricke, B.; Hammouche, A.; Linzen, D.; Thele, M.; Sauer, D.U. Impedance measurements on lead–acid batteries for state-of-charge, state-of-health and cranking capability prognosis in electric and hybrid electric vehicles. *J. Power Sources* **2005**, *144*, 418–425. [[CrossRef](#)]
20. Okoshi, T.; Yamada, K.; Hirasawa, T.; Emori, A. Battery condition monitoring (BCM) technologies about lead–acid batteries. *J. Power Sources* **2006**, *158*, 874–878. [[CrossRef](#)]
21. Zhang, X.; Grube, R.; Shin, K.K.; Salman, M.; Conell, R.S. Parity-relation-based state-of-health monitoring of lead acid batteries for automotive applications. *Control. Eng. Pract.* **2011**, *19*, 555–563. [[CrossRef](#)]
22. Ushiyama, K.; Morimoto, M. SOH estimation of lead acid battery for automobile. In Proceedings of the 2011 IEEE Ninth International Conference on Power Electronics and Drive Systems, Singapore, 5–8 December 2011; pp. 739–744. [[CrossRef](#)]
23. Marcos, J.; Cao-Paz, A.; Lago, A.; Nogueiras, A.; Peñalver, C. Fiber optic sensors for diagnosis and maintenance in lead-acid batteries. *IFAC Proc. Vol.* **2012**, *45*, 85–90. [[CrossRef](#)]
24. Li, Y.; Shen, Z.; Ray, A.; Rahn, C.D. Real-time estimation of lead-acid battery parameters: A dynamic data-driven approach. *J. Power Sources* **2014**, *268*, 758–764. [[CrossRef](#)]
25. Li, Y.; Chattopadhyay, P.; Ray, A.; Rahn, C.D. Identification of the battery state-of-health parameter from input–Output pairs of time series data. *J. Power Sources* **2015**, *285*, 235–246. [[CrossRef](#)]
26. Kerley, R.; Hyun, J.H.; Ha, D.S. Automotive lead-acid battery state-of-health monitoring system. In Proceedings of the IECON 2015—41st Annual Conference of the IEEE Industrial Electronics Society, Yokohama, Japan, 9–12 November 2015; pp. 003934–003938. [[CrossRef](#)]
27. Piłatowicz, G.; Budde-Meiwes, H.; Kowal, J.; Sarfert, C.; Schoch, E.; Königsmann, M.; Sauer, D.U. Determination of the lead-acid battery’s dynamic response using Butler-Volmer equation for advanced battery management systems in automotive applications. *J. Power Sources* **2016**, *331*, 348–359. [[CrossRef](#)]
28. Hyun, J.H. State of Health Estimation System for Lead-Acid Car Batteries Through Cranking Voltage Monitoring. Ph.D. Thesis, Virginia Tech, Blacksburg, VA, USA, 2016.
29. Bressanini, G.L.; Busarello, T.D.C.; Péres, A. Design and implementation of lead-acid battery state-of-health and state-of-charge measurements. In Proceedings of the 2017 Brazilian Power Electronics Conference (COBEP), Juiz de Fora, Brazil, 19–22 November 2017; pp. 1–6. [[CrossRef](#)]
30. Kwicien, M.; Schröer, P.; Kuipers, M.; Sauer, D. 4—Current research topics for lead–acid batteries. In *Lead-Acid Batteries for Future Automobiles*; Garche, J., Karden, E., Moseley, P.T., Rand, D.A., Eds.; Elsevier: Amsterdam, the Netherlands, 2017; pp. 133–146. [[CrossRef](#)]
31. Zhang, Y.; Du, X.; Salman, M. Battery state estimation with a self-evolving electrochemical ageing model. *Int. J. Electr. Power Energy Syst.* **2017**, *85*, 178–189. [[CrossRef](#)]
32. Kumar, B.; Khare, N.; Chaturvedi, P. FPGA-based design of advanced BMS implementing SoC/SoH estimators. *Microelectron. Reliab.* **2018**, *84*, 66–74. [[CrossRef](#)]
33. Wassiliadis, N.; Adermann, J.; Frericks, A.; Pak, M.; Reiter, C.; Lohmann, B.; Lienkamp, M. Revisiting the dual extended Kalman filter for battery state-of-charge and state-of-health estimation: A use-case life cycle analysis. *J. Energy Storage* **2018**, *19*, 73–87. [[CrossRef](#)]
34. Khaleghi, S.; Firouz, Y.; Van Mierlo, J.; Van den Bossche, P. Developing a real-time data-driven battery health diagnosis method, using time and frequency domain condition indicators. *Appl. Energy* **2019**, *255*, 113813. [[CrossRef](#)]
35. Li, W.; Rentemeister, M.; Badedda, J.; Jöst, D.; Schulte, D.; Sauer, D.U. Digital twin for battery systems: Cloud battery management system with online state-of-charge and state-of-health estimation. *J. Energy Storage* **2020**, *30*, 101557. [[CrossRef](#)]
36. Calborean, A.; Bruj, O.; Murariu, T.; Morari, C. Resonance frequency analysis of lead-acid cells: An EIS approach to predict the state-of-health. *J. Energy Storage* **2020**, *27*, 101143. [[CrossRef](#)]
37. Guida, G.; Faverato, D.; Colabella, M.; Buonomo, G. Robust state of charge and state of health estimation for batteries using a novel multi model approach. *Control. Theory Technol.* **2022**, *20*, 418–438. [[CrossRef](#)]
38. Dong, G.; Wei, J.; Zhang, C.; Chen, Z. Online state of charge estimation and open circuit voltage hysteresis modeling of LiFePO<sub>4</sub> battery using invariant imbedding method. *Appl. Energy* **2016**, *162*, 163–171. [[CrossRef](#)]
39. Baroi, S.; Sarker, P.C.; Baroi, S. An Improved MPPT Technique – Alternative to Fractional Open Circuit Voltage Method. In Proceedings of the 2017 2nd International Conference on Electrical & Electronic Engineering (ICEEE), Rajshahi, Bangladesh, 27–29 December 2017; pp. 1–4. [[CrossRef](#)]
40. Movassagh, K.; Raihan, A.; Balasingam, B.; Pattipati, K. A critical look at coulomb counting approach for state of charge estimation in batteries. *Energies* **2021**, *14*, 4074. [[CrossRef](#)]
41. Chang, W.Y. The state of charge estimating methods for battery: A review. *Int. Sch. Res. Not.* **2013**, *2013*, 953792. [[CrossRef](#)]

42. Xie, J.; Ma, J.; Bai, K. Enhanced coulomb counting method for state-of-charge estimation of lithium-ion batteries based on peukert's law and coulombic efficiency. *J. Power Electron.* **2018**, *18*, 910–922.
43. Lim, K.; Bastawrous, H.A.; Duong, V.H.; See, K.W.; Zhang, P.; Dou, S.X. Fading Kalman filter-based real-time state of charge estimation in LiFePO<sub>4</sub> battery-powered electric vehicles. *Appl. Energy* **2016**, *169*, 40–48. [[CrossRef](#)]
44. Shrivastava, P.; Soon, T.K.; Idris, M.Y.I.B.; Mekhilef, S. Overview of model-based online state-of-charge estimation using Kalman filter family for lithium-ion batteries. *Renew. Sustain. Energy Rev.* **2019**, *113*, 109233. [[CrossRef](#)]
45. Lee, G.; Kwon, D.; Lee, C. A convolutional neural network model for SOH estimation of Li-ion batteries with physical interpretability. *Mech. Syst. Signal Process.* **2023**, *188*, 110004. [[CrossRef](#)]
46. Jiang, S.; Song, Z. A review on the state of health estimation methods of lead-acid batteries. *J. Power Sources* **2022**, *517*, 230710. [[CrossRef](#)]
47. Tong, S.; Lacap, J.H.; Park, J.W. Battery state of charge estimation using a load-classifying neural network. *J. Energy Storage* **2016**, *7*, 236–243. [[CrossRef](#)]
48. Zebende, G.F. DCCA cross-correlation coefficient: Quantifying level of cross-correlation. *Phys. A Stat. Mech. Its Appl.* **2011**, *390*, 614–618. [[CrossRef](#)]
49. Peng, C.K.; Buldyrev, S.V.; Havlin, S.; Simons, M.; Stanley, H.E.; Goldberger, A.L. Mosaic organization of DNA nucleotides. *Phys. Rev.* **1994**, *49*, 1685. [[CrossRef](#)]
50. Podobnik, B.; Stanley, H.E. Detrended Cross-Correlation Analysis: A New Method for Analyzing Two Nonstationary Time Series. *Phys. Rev. Lett.* **2008**, *100*, 084102. [[CrossRef](#)] [[PubMed](#)]
51. Azevedo, G.A.; Sampaio, R.R.; Filho, A.S.N.; Moret, M.A.; Murari, T.B. Sustainable urban mobility analysis for elderly and disabled people in São Paulo. *Sci. Rep.* **2021**, *11*, 791. [[CrossRef](#)] [[PubMed](#)]
52. Figueiredo, P.; Moret, M.; Pascutti, P.; Nogueira, E., Jr.; Coutinho, S. Self-affine analysis of protein energy. *Phys. A Stat. Mech. Its Appl.* **2010**, *389*, 2682–2686. [[CrossRef](#)]
53. Santos, J.; Moreira, D.; Moret, M.; Nascimento, E. Analysis of long-range correlations of wind speed in different regions of Bahia and the Abrolhos Archipelago, Brazil. *Energy* **2019**, *167*, 680–687. [[CrossRef](#)]
54. Nascimento Filho, A.; Pereira, E.; Ferreira, P.; Murari, T.B.; Moret, M.A. Cross-correlation analysis on Brazilian gasoline retail market. *Phys. A Stat. Mech. Its Appl.* **2018**, *508*, 550–557. [[CrossRef](#)]
55. Murari, T.B.; Nascimento Filho, A.S.; Pereira, E.J.; Ferreira, P.; Pitombo, S.; Pereira, H.B.B.; Santos, A.A.; Moret, M.A. Comparative analysis between hydrous ethanol and gasoline c pricing in brazilian retail market. *Sustainability* **2019**, *11*, 4719. [[CrossRef](#)]
56. Ferreira, P.; Pereira, É.J.d.A.L.; da Silva, M.F.; Pereira, H.B.B. Detrended correlation coefficients between oil and stock markets: The effect of the 2008 crisis. *Phys. A Stat. Mech. Its Appl.* **2019**, *517*, 86–96. [[CrossRef](#)]
57. Pereira, E.J.d.A.L.; da Silva, M.F.; da Cunha Lima, I.; Pereira, H.B.B. Trump's Effect on stock markets: A multiscale approach. *Phys. A Stat. Mech. Its Appl.* **2018**, *512*, 241–247. [[CrossRef](#)]
58. Pereira, E.J.; Ferreira, P.; da Cunha Lima, I.C.; Murari, T.B.; Moret, M.A.; Pereira, H.B.B. Conservation in the Amazon rainforest and Google searches: A DCCA approach. *PLoS ONE* **2022**, *17*, e0276675. [[CrossRef](#)]
59. Azevedo, S.; Saba, H.; Miranda, J.; Filho, A.N.; Moret, M. Self-affinity in the dengue fever time series. *Int. J. Mod. Phys. C* **2016**, *27*, 1650143. [[CrossRef](#)]
60. Filho, A.S.N.; Murari, T.B.; Ferreira, P.; Saba, H.; Moret, M.A. A spatio-temporal analysis of dengue spread in a Brazilian dry climate region. *Sci. Rep.* **2021**, *11*, 11892. [[CrossRef](#)]
61. Oliveira, J.B.; Murari, T.B.; Nascimento Filho, A.S.; Saba, H.; Moret, M.A.; Cardoso, C.A.L. Paradox between adequate sanitation and rainfall in dengue fever cases. *Sci. Total. Environ.* **2023**, *860*, 160491. [[CrossRef](#)] [[PubMed](#)]
62. Kristoufek, L. Measuring correlations between non-stationary series with DCCA coefficient. *Phys. A Stat. Mech. Its Appl.* **2014**, *402*, 291–298. [[CrossRef](#)]
63. Dong, K.; Gao, Y.; Jing, L. Correlation tests of the engine performance parameter by using the detrended cross-correlation coefficient. *J. Korean Phys. Soc.* **2015**, *66*, 539–543. [[CrossRef](#)]
64. Piao, L.; Fu, Z. Quantifying distinct associations on different temporal scales: Comparison of DCCA and Pearson methods. *Sci. Rep.* **2016**, *6*, 1–11. [[CrossRef](#)] [[PubMed](#)]
65. Podobnik, B.; Jiang, Z.Q.; Zhou, W.X.; Stanley, H.E. Statistical tests for power-law cross-correlated processes. *Phys. Rev. E* **2011**, *84*, 066118. [[CrossRef](#)] [[PubMed](#)]

**Disclaimer/Publisher's Note:** The statements, opinions and data contained in all publications are solely those of the individual author(s) and contributor(s) and not of MDPI and/or the editor(s). MDPI and/or the editor(s) disclaim responsibility for any injury to people or property resulting from any ideas, methods, instructions or products referred to in the content.